

Investigating the Molecular Orientation and Thermal Stability of Spiro-OMeTAD and its Dopants by Near Edge X-Ray Absorption Fine Structure

Anita Brady-Boyd,* Kerry Hazeldine, Rachel E. Cross, Gongxizi Ren, Arthur Connell, Christopher P. Kershaw, Peter J. Holliman, and D. Andrew Evans

This study describes the utilization of near edge X-ray absorption fine structure (NEXAFS) to investigate the hole transporting material (HTM) 2,2',7,7'-tetrakis(*N,N*-di-*p*-methoxyphenylamine)-9,9'-spirobifluorene (Spiro-OMeTAD) and its most common dopants, lithium bis-(trifluoromethylsulfonyl) imide (LiTFSI), 4-*tert*-butylpyridine (*t*BP), and 2,3,5,6-tetrafluoro-7,7,8,8-tetracyanoquinodimethane (F4-TCNQ). By changing the angle of the sample with respect to the beam, the orientation of the molecules on the surface can be observed. The data suggest that it is difficult to determine any orientational preference for Spiro-OMeTAD deposited on a surface due to the 3D propeller-like geometry of this molecule. Both doped and undoped samples show thermal stability beyond the glass transition temperature of the molecules. Significant changes to the Spiro-OMeTAD spectra are observed with the addition of the dopants, in particular the C K-edge. Differences are also observed in the valence band spectra when dopants are added. It is also demonstrated how the doping combination of LiTFSI with *t*BP and, F4-TCNQ act as p-type dopants by altering the position of the HOMO levels. The F4-TCNQ induces a larger change in the HOMO levels when compared to the LiTFSI and *t*BP. These results are important to increase the understanding of Spiro-OMeTAD and the effect dopants have on this material for next generation solar cells.

1. Introduction


Photovoltaic (PV) research has seen a paradigm shift in recent years through the introduction of organic-lead halide perovskite materials as light absorbers in PV devices, with current perovskite solar cells (PSCs) reaching a power conversion efficiency (PCE) of 25.7%.^[1–3] Perovskite-based solar cells are an attractive alternative to traditional silicon-based cells for a multitude of reasons including their high charge carrier mobilities, tunable bandgaps, wide spectral response, solution-based processing, long charge carrier diffusion lengths, and potential scalable fabrication.^[4–13] PSCs may also represent a significant cost reduction in terms of fabrication, with the aim of providing a cheaper substitute to silicon-based cells and ultimately a more sustainable alternative to fossil fuel electricity generation. Organic-lead halide perovskites, mainly methylammonium, formamidinium, or cesium (MPbX, where M = organic cation or Cs and X = I, Cl, Br) based,

have been the subject of immense research and have recorded some of the highest PCEs due to their efficacy as solar harvesting materials.^[14–17]

A vital component of the PSC is the HTM whose main purpose is to optimize the electronic properties at the interface between the perovskite layer and the electrode by efficient hole extraction. Efficient charge transfer within HTM films is strongly affected by molecular orientation, the degree of crystallinity, and film quality. Recent work has also shown the importance of molecular orientation in light-harvesting dyes in dye-sensitized solar cells.^[18,19] There are many variations of organic HTMs known, these can broadly be divided into families based on their core structure and include the “Spiro” HTMs^[20] and planar HTMs such as triazatruxene^[21] or triphenylamine (TPA).^[22,23] The most popular of these organic HTMs being the Spiro-OMeTAD that has been the subject of intense research since the late 1990s.^[24–28] The Spiro-OMeTAD films are generally doped by a combination of LiTFSI and *t*BP. This doping combination has proven itself to have a higher efficacy than undoped Spiro-OMeTAD films.

A. Brady-Boyd, K. Hazeldine, R. E. Cross, G. Ren, D. A. Evans
Department of Physics
Aberystwyth University
Aberystwyth SY23 3BZ, UK
E-mail: anb116@aber.ac.uk

A. Connell, C. P. Kershaw, P. J. Holliman
Faculty of Science and Engineering
Bay Campus
Swansea University
Swansea SA1 8EN, UK

 The ORCID identification number(s) for the author(s) of this article can be found under <https://doi.org/10.1002/apxr.202200045>

© 2023 The Authors. Advanced Physics Research published by Wiley-VCH GmbH. This is an open access article under the terms of the Creative Commons Attribution License, which permits use, distribution and reproduction in any medium, provided the original work is properly cited.

DOI: 10.1002/apxr.202200045

Whilst the doping of Spiro-OMeTAD with LiTFSI+*t*BP has a positive outcome on PCEs these materials also have their limitations. The function of LiTFSI has been reported to be to oxidize the Spiro-OMeTAD which dramatically increases the hole conductivity.^[29] However, direct oxidation seems unlikely because LiTFSI is not an oxidizing agent. Unfortunately, the LiTFSI is hygroscopic and readily absorbs water causing the degradation of the perovskite. Originally, the *t*BP was used to prevent contact between the mesoporous TiO₂ and the Spiro-OMeTAD. It has been discovered however that the *t*BP serves to inhibit aggregation of the LiTFSI thereby improving its dispersion throughout the hole transporting layer (HTL), as well as reducing the number of pinholes that form on the surface. Thus forming a much more homogenous HTL film.^[30,31] The *t*BP has been reported to chemically interact with the perovskite and creates a p-doped region at the perovskite/*t*BP interface.^[32] Although the efficiency is seen to increase initially, long term, *t*BP has detrimental effects on devices. *t*BP is actually corrosive to the perovskite layer, as it dissolves the PbI₂ which serves to decompose the perovskite.^[33] Following thermal stress, *t*BP can also cause de-doping of the Spiro-OMeTAD through a complex process where the Spiro-OMeTAD reverts to its unoxidized state.^[34,35]

Therefore, alternative dopants to LiTFSI+*t*BP are required that must not only retain the positive attributes of the LiTFSI+*t*BP complex but improve upon them and promote higher PCEs for perovskite devices. To generate any improvement, replacement dopants for LiTFSI+*t*BP would need to prohibit moisture infiltrating the device and degrading the perovskite as well as possessing enhanced atmospheric stability and sustainable long-life efficiencies. When used with Spiro-OMeTAD, vacuum-deposited F4-TCNQ has been found to create pinhole-free films that exhibit improved air stability and sustained PCEs over 810 hours, when compared to spin-coated Spiro-OMeTAD films.^[36,37] F4-TCNQ is non-hygroscopic so will not degrade the perovskite and it is also compatible with solution-based processing.^[38] These properties make F4-TCNQ an outstanding candidate to replace LiTFSI+*t*BP as the dopant of choice for Spiro-OMeTAD films.

In this study, we utilize NEXAFS along with valence band spectra and DFT to examine, contrast and compare Spiro-OMeTAD, Spiro-OMeTAD+LiTFSI+*t*BP, and Spiro-OMeTAD+F4-TCNQ. NEXAFS is known for revealing a materials unique chemical “fingerprint” as the technique is very sensitive to bonding environment. Therefore, even in complex molecules like Spiro-OMeTAD, NEXAFS can distinguish the local bonding environment. NEXAFS is highly polarization dependent, and synchrotrons produce radiation beams that are highly polarized. Large complex molecules like Spiro-OMeTAD will have resonances associated with both σ^* and π^* resonances which have a strong and opposite polarization dependence. Consequently, utilizing NEXAFS permits the investigation of the orientation of the Spiro-OMeTAD on the surface by simply changing the angle of the sample with respect to the beam. Despite its importance, molecular orientation within HTM films is poorly understood and so we studied spin-coated Spiro-OMeTAD, Spiro-OMeTAD+LiTFSI+*t*BP, and Spiro-OMeTAD+F4-TCNQ films to investigate this property. Doped Spiro-OMeTAD films are probed with the purpose to detect any variation in the molecular orientation and thermal stability, and to access their influence on the Spiro-OMeTAD spectra.

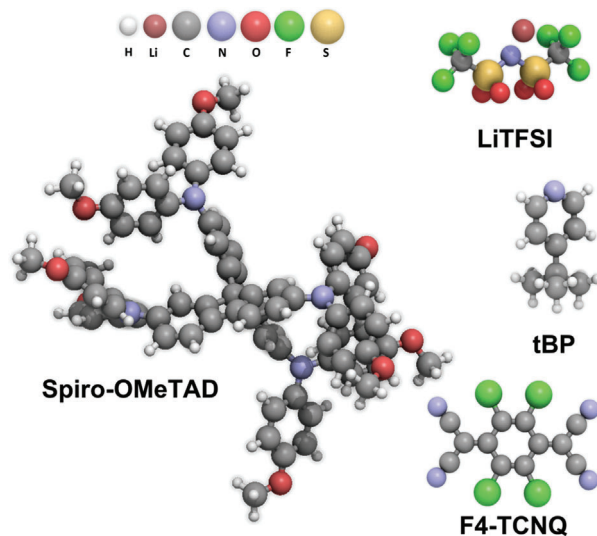


Figure 1. Spiro-OMeTAD and the dopants of interest in this study, LiTFSI+*t*BP, and F4-TCNQ. Molecule diagrams generated by Qutemol.^[41]

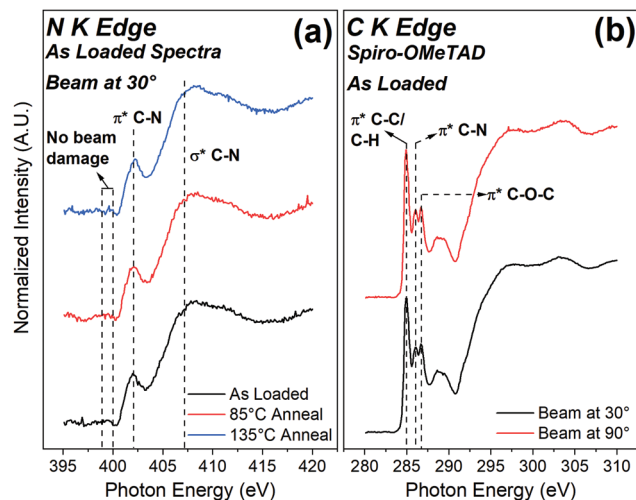


Figure 2. a) Nitrogen K-edge of Spiro-OMeTAD showing the molecules thermal stability up to 135 °C and no visible beam damage b) carbon K-edge shows no determinable preferred orientation.

2. Results and Discussion

The structure of each molecule is shown in Figure 1. The complex geometry of the Spiro-OMeTAD is shown in more detail in Video S1 (Supporting Information). The undoped Spiro-OMeTAD is used as the reference sample to compare any observed changes in the doped samples. C K-edge NEXAFS spectra of the Spiro-OMeTAD show three distinct peaks at 285.0, 286.1, and 286.8 eV, displayed in Figure S1 (Supporting Information). These peaks can be attributed to the three distinct bonding environments of carbon within the molecule that are C-C/C-H bonds, C-N bonds,^[39] and C-O-C bonds,^[40] respectively.

To assess the extent to which these films are thermally stable, they received cumulative in situ anneals up to 135 °C. The N K-edge, Figure 2a, displays the thermal stability of the undoped Spiro-OMeTAD molecule because there are no observable

differences between the as-loaded spectra and the subsequent anneals. This is also observed in the C K-edge (Figure S2, Supporting Information). From this N K-edge data, we can also dismiss the possibility of beam damage. Previous studies have shown that the C–N bonds found in common materials including polymers can be broken easily when exposed to ionizing radiation.^[42] This results in two characteristic peaks in N K-edge spectra at photon energies of 398.9 and 400.0 eV. These peaks are absent from our spectra showing there is no beam damage. This is due to several reasons i) the low flux at the beamline (1×10^{11} photon s^{-1}), ii) no prolonged exposure to the synchrotron beam (sample position was moved before each scan set was recorded), and finally, iii) the propeller-like shape of the Spiro-OMeTAD molecule itself essentially offering some protection to the N–C bond. Since all the nitrogen present in the Spiro-OMeTAD is in the same chemical state, the visible peak at 402.0 eV and the broad region from ≈ 407.0 eV have been assigned to π^* and σ^* resonances of C–N bonds, respectively. It is also worth noting that the N K-edge is virtually indistinguishable from that of a triphenylamine (TPA) molecule given that diphenylamine moieties are the peripheral donor ligands of Spiro-OMeTAD.^[39]

Figure 2b presents the C K-edge for the Spiro-OMeTAD taken at two different angles with respect to the beam, 30° (least surface sensitive) and 90° (most surface sensitive, according to Figure S3, Supporting Information). There is no change observed in the spectra elucidating that there is no apparent preferred orientation of the Spiro-OMeTAD molecule in these films. These findings are interesting when compared to the data reported by Shibayama et al. who observed some orientation of Spiro-OMeTAD layers when deposited on certain substrates (i.e., Si, FTO, nickel oxide, and perovskite layers).^[43] They demonstrated there is variation in Spiro-OMeTAD behavior from substrate to substrate and they suggested that Spiro-OMeTAD orientation was influenced by substrate surface energy. However, their study did not investigate Spiro-OMeTAD deposited on TiO_2 and so the authors believe the data reported here are the first reported on this substrate. In addition, there is no observed change in the Spiro-OMeTAD spectra with applied temperature, there is no observable beam damage and finally, there appears to be no distinguishable preferred orientation of the molecule when deposited. Spin-coating appears to have produced high-quality films as all the spectra are reproducible even when taken at different positions across the surface.

With the addition of the dopants, several changes are noticeable in the C K-edge spectra as shown in Figure 3a. In the Spiro-OMeTAD+LiTFSI+*t*BP sample, a change is noticed in the peak at 286.8 eV which is the C–O–C peak. This increase can be attributed to oxidation of the Spiro-OMeTAD by atmospheric oxygen. This oxidation is accelerated in the presence of the dopants because they disrupt the packing of the Spiro-OMeTAD molecules making the film more porous which increases the rate of O_2 diffusion which is otherwise known to be slow.^[44] There is also a pre-edge feature present that is indicative of C=O bonds again owing to the oxidizing effect this dopant has on the Spiro-OMeTAD. The peak at 285.0 eV sees a decrease in intensity due to the LiTFSI molecules lying near the top interface.^[30] The F4-TCNQ has four C \equiv N bonds (Figure 1) and these are the source of the increase in the 286.1 eV peak in Figure 3a, for the Spiro-OMeTAD+F4-TCNQ sample. There does not appear to

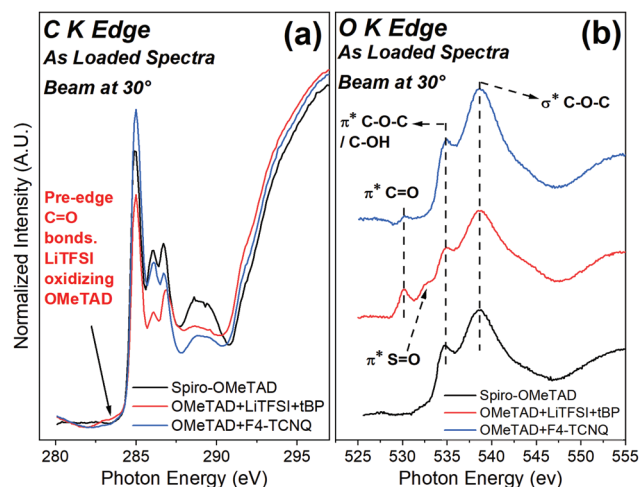


Figure 3. a) Carbon K-edge and b) oxygen K-edge spectra showing the influence of the dopants on the Spiro-OMeTAD.

be any noticeable pre-edge feature for the Spiro-OMeTAD+F4-TCNQ sample but from the O K-edge (Figure 3b) a small peak corresponding to C=O bonds is visible. This implies that the F4-TCNQ might also indirectly contribute some oxidizing effect on the Spiro-OMeTAD by again disrupting the Spiro-OMeTAD molecules to increase the rate of O_2 diffusion into the films. However, the effect for F4-TCNQ is less than for LiTFSI+*t*BP because there is only one dopant molecule here so the disruption of the Spiro-OMeTAD molecules is expected to be less. An increase in intensity can be seen for the 285.0 eV peak as the F4-TCNQ contributes to this peak. Considering that the dopants only account for a small weight percentage of the overall layer these changes in the C K-edge spectra are significant. The O K-edge of the three samples displayed in Figure 3b emulates these findings. The emergence of a C=O peak at 530.1 eV^[45] in the Spiro-OMeTAD+LiTFSI+*t*BP again shows the increase in atmospheric oxidation indirectly caused by the LiTFSI+*t*BP increasing the porosity of the Spiro-OMeTAD film. Also visible is a peak at 532.6 eV corresponding to S=O bonds in the LiTFSI molecule. The Spiro-OMeTAD+F4-TCNQ sample shares a strong resemblance to the Spiro-OMeTAD.

Interestingly, both doped samples show the same level of thermal stability as the Spiro-OMeTAD with no evident change in the spectra with annealing, Figure 4a. This indicates that the dopants do not compromise the thermal properties of the Spiro-OMeTAD. Investigating the orientation of the doped samples we find that again there is no evidence for preferred orientation. For the Spiro-OMeTAD+F4-TCNQ, this is shown in the N K-edge Figure 4b. This is not surprising as i) the F4-TCNQ should be homogeneously distributed throughout the layer and (ii) although we observe the changes in the spectra when the dopants are added these changes are subtle. The Spiro-OMeTAD accounts for $\approx 70\%$ (wt.) of the HTL so any changes in orientation of the dopants would likely be very small and difficult to observe in the recorded spectra. The emergence of a peak at 398.9 eV has been assigned to the C \equiv N bonds from the F4-TCNQ.^[46] However, the Spiro-OMeTAD+LiTFSI+*t*BP does show some differences with a change of angle (Figure S4, Supporting Information). This is

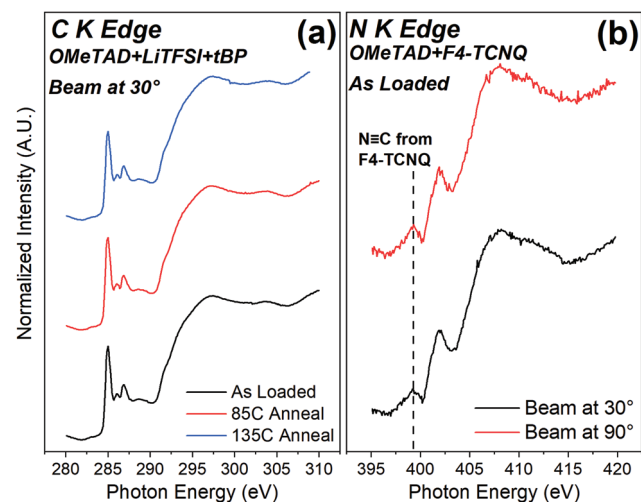


Figure 4. a) Carbon K-edge for the OMeTAD+LiTFSI+tBP sample exhibits good thermal stability b) nitrogen K-edge shows no change in the spectra at different angles.

expected as the LiTFSI molecules are known to agglomerate and tend to be more surface localized leading to a more inhomogeneous layer.^[30,47] While the emergence of a peak at 288.1 eV assigned to COOH, is detected.^[48] This is further evidence of the indirect increase in atmospheric oxidation that the LiTFSI+tBP dopants have on the Spiro-OMeTAD. It could also be the key to its hygroscopic nature as strongly polar groups are known to attract water molecules.

A wealth of information can be obtained from the UPS including the secondary cut-off, the work function, and the ionization potential which helps us build a picture of the HOMO levels of the Spiro-OMeTAD. The UPS spectra are used to find a common scale to compare our synchrotron valence bands for the Spiro-OMeTAD. In the Supporting Information, a detailed account is given of how the HOMO levels of an organic molecule on a metallic substrate can be determined. It cannot be assumed that the vacuum level is the same for the substrate and the organic and so this needs to be taken into account when calculating the HOMO levels.^[49,50] It is worth noting that for the UPS, the Spiro-OMeTAD was deposited on Ti foil with a thick TiO₂ layer, to negate any charging effects, as charging was observed with the ITO glass substrates. In Figure S5a (Supporting Information), the UPS spectra of the reference TiO₂ and the Spiro-OMeTAD are displayed, while Figure S5b (Supporting Information) shows the XPS of the Ti 2p region. Figure S6 (Supporting Information) uses the method from Ishii and Seki^[50] to find the HOMO level for the UPS spectra as well as the synchrotron spectra. It can be seen that the spectra are practically identical from the two different measurement techniques. The obtained value for the HOMO level of the Spiro-OMeTAD was found to be 5.42 eV for both samples. Unfortunately, this method cannot be performed for all the data here as we are missing the secondary cut offs for the synchrotron samples. Using the vacuum level difference for the undoped Spiro-OMeTAD would not suffice for the doped samples and would lead to inaccurate assignments for the HOMO levels. Instead, as shown in Figure 5a, we reference all samples to the Fermi level and not the vacuum level. In this way, a comparative

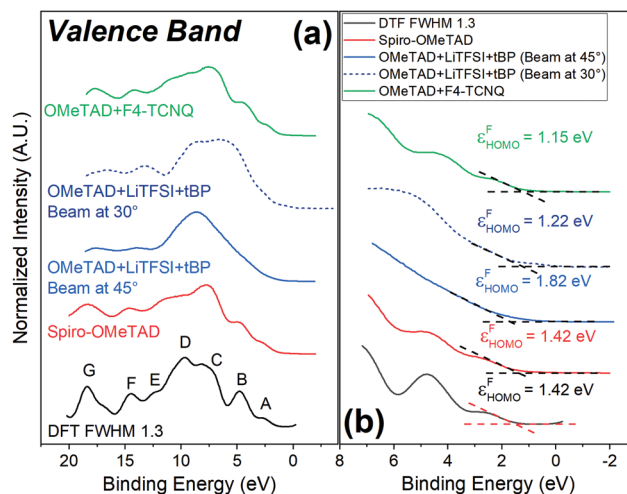


Figure 5. a) Valence band spectra show similarities between the DFT calculated spectra and the experimental Spiro-OMeTAD and the OMeTAD+F4-TCNQ samples. The Spiro-OMeTAD+LiTFSI+tBP sample on the other hand is distinct b) ϵ_{HOMO}^F levels of the different samples.

analysis can still be performed on the HOMO levels referenced to the Fermi level (ϵ_{HOMO}^F), as any shifts in energy between the samples are real shifts, although the energy scale is not absolute.^[36]

Valence band spectra in Figure 5a were taken at a photon energy of 130 eV and allow for an extremely surface-sensitive measurement of only the top couple of nanometers. For this reason, the spectra were taken so that the electron emission was normal with respect to the position of the electron energy analyzer, or the angle between the sample and the beam was 45°, as shown in Figure S3 (Supporting Information). This configuration allowed for the deepest sampling depth, while still allowing surface sensitivity. As confirmed by photoemission Survey spectra, recorded alongside the valence band spectra, there is no signal detected from the underlying TiO₂ (Figure S7, Supporting Information). Also shown in Figure 5a is the DFT calculated spectra for the Spiro-OMeTAD with the main contribution bands labeled A-G. The calculated and measured Spiro-OMeTAD spectra agree very well and have the same overall shape. The ϵ_{HOMO}^F for both is observed to be the same at 1.42 eV, which is in good agreement with the literature, Figure 5b.^[36] The shape of the Spiro-OMeTAD+LiTFSI+tBP is different from the Spiro-OMeTAD and the Spiro-OMeTAD+F4-TCNQ samples. The bands labeled A, B, and G, which are characteristic of the Spiro-OMeTAD film are not visibly present in the Spiro-OMeTAD+LiTFSI+tBP sample. Arguably, the broad area could be a convolution of bands C and D. While a small contribution from band F is observed. Once again pointing to an interface that is inhomogeneous due to the dopants.

As the initial Spiro-OMeTAD+LiTFSI+tBP spectra were not as expected, valence band spectra were also recorded at a different angle along with the NEXAFS spectra, as seen in the dashed line in Figure 5a,b. It is observed how the line shape changes as the angle changes. Although the main role of the tBP is to disperse the LiTFSI within the Spiro-OMeTAD film it is not fully effective, and some agglomerations do still persist leading to an inhomogeneous surface.^[30] When the beam is at 30° with respect to the

sample, its shape is more similar to the other two samples. The Spiro-OMeTAD contributions from the bands start to become visible, showing mixing of the Spiro-OMeTAD with the LiTFSI+tBP dopants. However, when the beam is at 45° with respect to the sample this similarity in shape is not observed. The position of the sample was regularly changed to avoid beam damage, this coupled with the increased surface sensitivity of the valence band measurements lead the authors to believe that at this 45° angle, the spectra is at an inhomogeneous region of the surface.

The other two samples are very similar, and this mirrors what is observed in the NEXAFS spectra. The Spiro-OMeTAD and the Spiro-OMeTAD+F4-TCNQ samples have similar spectral shapes with only slight differences which are due to the F4-TCNQ dopant. This again suggests that F4-TCNQ is most likely homogeneously distributed throughout the sample in a solid solution.

Another interesting point to note from the valence band spectra is the ϵ_{HOMO}^F positions. The Spiro-OMeTAD+F4-TCNQ has a ϵ_{HOMO}^F of 1.15 eV. The combination of LiTFSI+tBP is generally thought of as a good p-type dopant that can enhance the hole conductivity, due to its indirect oxidizing effect on the Spiro-OMeTAD. For the area of the surface where there was homogeneous distribution of the Spiro-OMeTAD and the LiTFSI+tBP dopants, a p-type behavior was observed and the ϵ_{HOMO}^F was at 1.22 eV. However, when the sample is at the inhomogeneous region of the surface the ϵ_{HOMO}^F is observed at a higher binding energy position of 1.82 eV. The Spiro-OMeTAD+F4-TCNQ has a lower ϵ_{HOMO}^F than the undoped Spiro-OMeTAD and the Spiro-OMeTAD+LiTFSI+tBP making it more p-type and a more efficient HTM, consistent with previous observations.^[36]

3. Conclusion

In conclusion, using NEXAFS, the orientation of the Spiro-OMeTAD molecule within the HTL has been investigated. The complex 3D structure of the Spiro-OMeTAD shows no preferred orientation as the spectra taken at different angles appear indistinguishable. The Spiro-OMeTAD is thermally stable up to 135 °C and stable under the synchrotron beam showing no signs of decomposition. We have also investigated the consequences of adding different dopants on the Spiro-OMeTAD. The LiTFSI+tBP dopants exert an indirect effect of increasing atmospheric oxidation by disrupting the Spiro-OMeTAD molecules within the film which increase film porosity. This is apparent in the C K-edge with i) an increase in the C—O—C component peak, ii) the emergence of a pre-edge feature which is indicative of C=O bonds, and iii) a new peak at 288.1 eV, attributed to COOH, becomes visible when the angle of the beam is at 90° (increased surface sensitivity). With the introduction of F4-TCNQ to the Spiro-OMeTAD an increase is seen in the C≡N component peak of the C K-edge. A peak also appears in the N K-edge owing to the C≡N bonds in the F4-TCNQ. Both dopants show excellent thermal stability up to 135 °C and resistance to beam damage. Valence band spectra reveal that the ϵ_{HOMO}^F for the Spiro-OMeTAD+LiTFSI+tBP (when the dopants are homogenous) moves to a lower binding energy indicating that this dopant induces a p-type doping effect in the material. While the ϵ_{HOMO}^F of the Spiro-OMeTAD+F4-TCNQ has an even lower binding energy indicating that this dopant in-

duces a larger p-type effect in the material. This work demonstrates that F4-TCNQ is an excellent potential replacement for LiTFSI+tBP as the dopant used with Spiro-OMeTAD. The F4-TCNQ does not disrupt the Spiro-OMeTAD molecules as much as LiTFSI+tBP that keeps film porosity lower, and it does not retain moisture that could extend the lifetimes of perovskite devices. Finally, as the valence bands show, the F4-TCNQ brings the ϵ_{HOMO}^F closer to the Fermi level allowing for more efficient hole transport.

4. Experimental Section

Sample Preparation: Indium tin oxide (ITO) covered glass ≈3 mm thick, was coated in a compact TiO₂ layer. 70 mg mL⁻¹ of the synthesized Spiro-OMeTAD, (Ossila, 99.8%, unsublimed) was dissolved in anhydrous chlorobenzene (1 mL). Two sets of additives were added to the chlorobenzene Spiro-OMeTAD solution. In one set, tris(bis(trifluoromethylsulfon-yl) imide) (Sigma; Li-TFSI, 25 mol%) was added from a 1.8 M stock solution in CH₃CN along with *tert*-butylpyridine (Sigma; tBP, 12.5 mol.%). In the second set, 7,7,8,8-tetracyano-2,3,5,6-tetrafluoroquinodimethane (Sigma, F4-TCNQ, 12.5 mol%) was added. The final HTM solutions were spin-coated onto the TiO₂ layers at 2000 rpm for 45 s yielding a thick film (≈100 nm) that visibly covered the entire substrate. For UPS measurements, the Spiro-OMeTAD was deposited on TiO₂ foil using an in vacuo evaporation method. The Spiro-OMeTAD was placed on the substrate using a pipette and was dried by slowly turning on the roughing vacuum for the UPS load lock. This process quickly removed the solvent and stopped a thick contamination layer from forming on the Spiro-OMeTAD.

Near Edge X-Ray Fine Structure: Total electron yield (TEY) NEXAFS measurements were performed on the MATLINE beamline at the ASTRID II synchrotron in the University of Aarhus, Denmark. The usable photon energy range was from 20 to 700 eV allowing for the acquisition of the carbon, nitrogen, and oxygen K-edges. The base pressure of the system was ca. 4×10⁻¹⁰ mbar. Each sample received two in vacuo anneals at 85 and 135 °C corresponding to the maximum expected thermal budget of an installed solar cell and just above the glass transition temperature (T_g) of the Spiro-OMeTAD ($T_g = 125$ °C), respectively. The samples were kept at the dwell temperature for 1 h. For each sample, spectra were collected with the synchrotron beam incidence at two different angles with respect to the substrate, namely 30° and 90°. At each angle, the K-edge for the carbon, nitrogen, and oxygen were recorded. Any change in the spectra at the different angles would suggest a preferred orientation of the molecule. Following each angle change and anneal the scan position was changed to reduce any beam damage. The spectra were analyzed using Athena that is part of the Demeter software package, version 0.9.26, specifically designed for analysis of X-ray absorption spectra.^[51] All data were normalized using Athena's normalization procedure.

Valence Band—Experimental and Density Functional Theory: Valence band spectra were also taken at the same beamline all using a photon energy of 130 eV and a step size of 0.05 eV. The bands were recorded along with the NEXAFS at different angles and at 45° to the beam. Valence band data were recorded after each anneal as for the NEXAFS data and compared with valence band spectra recorded with a laboratory-based UPS. The laboratory-based UPS data were recorded using He I emission with a photon energy of 21.22 eV, a pass energy of 10 eV, a step size of 0.02 eV. The samples were calibrated to the Fermi edge of a reference TiO₂ foil. The DFT simulations were carried out using Gaussian 09 version D.01 software package to calculate the optimized molecular geometries of Spiro-OMeTAD.^[52] The ground state calculations were performed at B3LYP/6-31G(d,p) level in vacuum.

Supporting Information

Supporting Information is available from the Wiley Online Library or from the author.

Acknowledgements

The authors acknowledge the European Regional Development Fund (ERDF) and the Welsh European Funding Office (WEFO) for funding the second Solar Photovoltaic Academic Research Consortium (SPARC II) and the EPSRC (EP/M015254/2, EP/P030068/1), which supported this research. The research leading to this result has been supported by the project CALIPSOplus under Grant Agreement 730872 from the EU Framework Programme for Research and Innovation HORIZON 2020. The authors would like to thank Zheshen Li of Aarhus University for his help while at the beamline.

Conflict of Interest

The authors declare no conflict of interest.

Data Availability Statement

The data that support the findings of this study are available from the corresponding author upon reasonable request.

Keywords

F4-TCNQ, hole transporting materials, LiTFSI-tBP, near edge x-ray absorption fine structures, Spiro-OMeTAD, valence band

Received: September 22, 2022

Revised: March 22, 2023

Published online:

- [1] M. Jeong, I. W. Choi, E. M. Go, Y. Cho, M. Kim, B. Lee, S. Jeong, Y. Jo, H. W. Choi, J. Lee, J.-H. Bae, S. K. Kwak, D. S. Kim, C. Yang, *Science* **2020**, *369*, 1615.
- [2] M. A. Green, E. D. Dunlop, J. Hohl-Ebinger, M. Yoshita, N. Kopidakis, K. Bothe, D. Hinken, M. Rauer, X. Hao, *Prog. Photovoltaics Res. Appl.* **2022**, *30*, 687.
- [3] National Renewable Energy Laboratory, *Solar Cell Efficiencies* <https://www.nrel.gov/pv/cell-efficiency.html>. (accessed: September 2022).
- [4] G. Xing, N. Mathews, S. Sun, S. S. Lim, Y. M. Lam, M. Grätzel, S. Mhaisalkar, T. C. Sum, *Science* **2013**, *342*, 344.
- [5] S. D. Stranks, G. E. Eperon, G. Grancini, C. Menelaou, M. J. P. Alcocer, T. Leijtens, L. M. Herz, A. Petrozza, H. J. Snaith, *Science* **2013**, *342*, 341.
- [6] Y. Yang, J. You, Z. Hong, Q. Chen, M. Cai, T. Bin Song, C. C. Chen, S. Lu, Y. Liu, H. Zhou, *ACS Nano* **2014**, *8*, 1674.
- [7] E. Edri, S. Kirmayer, S. Mukhopadhyay, K. Gartsman, G. Hodes, D. Cahen, *Nat. Commun.* **2014**, *5*, 3461.
- [8] J. Haruyama, K. Sodeyama, L. Han, Y. Tateyama, *J. Am. Chem. Soc.* **2015**, *137*, 10048.
- [9] X. Huang, T. R. Paudel, P. A. Dowben, S. Dong, E. Y. Tsybal, *Phys. Rev. B* **2016**, *94*, 195309.
- [10] E. W. Jones, P. J. Holliman, A. Connell, M. L. Davies, J. Baker, R. J. Hobbs, S. Ghosh, L. Furnell, R. Anthony, C. Pleydell-Pearce, *Chem. Commun.* **2016**, *52*, 4301.
- [11] M.-W. Lin, K.-C. Wang, J.-H. Wang, M.-H. Li, Y.-L. Lai, T. Ohgashi, N. Kosugi, P. Chen, D.-H. Wei, T.-F. Guo, Y.-J. Hsu, *Adv. Mater. Interfaces* **2016**, *3*, 1600135.
- [12] P. J. Holliman, E. W. Jones, R. J. Hobbs, A. Connell, L. Furnell, R. Anthony, C. P. Kershaw, *Mater. Lett.: X* **2019**, *2*, 100011.
- [13] C. C. Chueh, C. Z. Li, A. K. Y. Jen, *Energy Environ. Sci.* **2015**, *8*, 1160.
- [14] R. A. Kerner, P. Schulz, J. A. Christians, S. P. Dunfield, B. Dou, L. Zhao, G. Teeter, J. J. Berry, B. P. Rand, *APL Mater.* **2019**, *7*, 041103.
- [15] H. Zhou, Q. Chen, G. Li, S. Luo, T.-b. Song, H.-S. Duan, Z. Hong, J. You, Y. Liu, Y. Yang, *Science* **2014**, *345*, 542.
- [16] A. Suzuki, H. Okada, T. Oku, *Energies* **2016**, *9*, 376.
- [17] M. Kim, G. H. Kim, T. K. Lee, I. W. Choi, H. W. Choi, Y. Jo, Y. J. Yoon, J. W. Kim, J. Lee, D. Huh, H. Lee, S. K. Kwak, J. Y. Kim, D. S. Kim, *Joule* **2019**, *3*, 2179.
- [18] P. J. Holliman, C. P. Kershaw, E. W. Jones, D. Meza-Rojas, A. Lewis, J. McGettrick, D. Geatches, K. Sen, S. Metz, G. J. Tizzard, S. J. Coles, *J. Mater. Chem. A* **2020**, *8*, 22191.
- [19] P. J. Holliman, M. Mohsen, A. Connell, C. P. Kershaw, D. Meza-Rojas, E. W. Jones, D. Geatches, K. Sen, Y. W. Hsiao, *Energies* **2020**, *13*, 4637.
- [20] X. Zhao, M. Wang, *Mater. Today Energy* **2018**, *7*, 208.
- [21] A. Connell, Z. Wang, Y.-H. Lin, P. C. Greenwood, A. A. Wiles, E. W. Jones, L. Furnell, R. Anthony, C. P. Kershaw, G. Cooke, H. J. Snaith, P. J. Holliman, *J. Mater. Chem. C* **2019**, *7*, 5235.
- [22] H. Choi, S. Paek, N. Lim, Y. H. Lee, M. K. Nazeeruddin, J. Ko, *Chem. – A Eur. J.* **2014**, *20*, 10894.
- [23] P. Agarwala, D. Kabra, *J. Mater. Chem. A* **2017**, *5*, 1348.
- [24] U. Bach, D. Lupo, P. Comte, J. E. Moser, F. Weissörtel, J. Salbeck, H. Spreitzer, M. Grätzel, *Nature* **1998**, *395*, 583.
- [25] S. Fantacci, F. De Angelis, M. K. Nazeeruddin, M. Grätzel, *J. Phys. Chem. C* **2011**, *115*, 23126.
- [26] L. K. Ono, P. Schulz, J. J. Endres, G. O. Nikiforov, Y. Kato, A. Kahn, Y. Qi, *J. Phys. Chem. Lett.* **2014**, *5*, 1374.
- [27] F. Hao, C. C. Stoumpos, D. H. Cao, R. P. H. Chang, M. G. Kanatzidis, *Nat. Photonics* **2014**, *8*, 489.
- [28] A. Barranco, M. C. Lopez-Santos, J. Idigoras, F. J. Aparicio, J. Obrero-Perez, V. Lopez-Flores, L. Contreras-Bernal, V. Rico, J. Ferrer, J. P. Espinos, A. Borrás, J. A. Anta, J. R. Sanchez-Valencia, *Adv. Energy Mater.* **2020**, *10*, 1901524.
- [29] A. Abate, T. Leijtens, S. Pathak, J. Teuscher, R. Avolio, M. E. Errico, J. Kirkpatrick, J. M. Ball, P. Docampo, I. McPherson, H. J. Snaith, *Phys. Chem. Chem. Phys.* **2013**, *15*, 2572.
- [30] E. J. Juarez-Perez, M. R. Leyden, S. Wang, L. K. Ono, Z. Hawash, Y. Qi, *Chem. Mater.* **2016**, *28*, 5702.
- [31] S. Wang, M. Sina, P. Parikh, T. Uekert, B. Shahbazian, A. Devaraj, Y. S. Meng, *Nano Lett.* **2016**, *16*, 5594.
- [32] S. N. Habisreutinger, N. K. Noel, H. J. Snaith, R. J. Nicholas, *Adv. Energy Mater.* **2017**, *7*, 1601079.
- [33] W. Li, H. Dong, L. Wang, N. Li, X. Guo, J. Li, Y. Qiu, *J. Mater. Chem. A* **2014**, *2*, 13587.
- [34] F. Lamberti, T. Gatti, E. Cescon, R. Sorrentino, A. Rizzo, E. Menna, G. Meneghesso, M. Meneghetti, A. Petrozza, L. Franco, *Chem* **2019**, *5*, 1806.
- [35] E. Kasparavicius, A. Magomedov, T. Malinauskas, V. Getautis, *Chem. – A Eur. J.* **2018**, *24*, 9910.
- [36] M. C. Jung, S. R. Raga, L. K. Ono, Y. Qi, *Sci. Rep.* **2015**, *5*, 9863.
- [37] M. C. Jung, Y. Qi, *Org. Electron. physics, Mater. Appl.* **2016**, *31*, 71.
- [38] J. Luo, C. Jia, Z. Wan, F. Han, B. Zhao, R. Wang, *J. Power Sources* **2017**, *342*, 886.
- [39] T. Zhang, I. E. Brumboiu, C. Grazioli, A. Guarnaccio, M. Coreno, M. De Simone, A. Santagata, H. Rensmo, B. Brena, V. Lanzilotto, C. Puglia, *J. Phys. Chem. C* **2018**, *122*, 17706.
- [40] O. Dhez, H. Ade, S. G. Urquhart, *J Electron Spectros Relat Phenomena* **2003**, *128*, 85.
- [41] M. Tarini, P. Cignoni, C. Montani, *IEEE Trans Vis Comput Graph* **2006**, *12*, 1237.
- [42] P. S. Johnson, P. L. Cook, X. Liu, W. Yang, Y. Bai, N. L. Abbott, F. J. Himpsel, *J. Chem. Phys.* **2011**, *135*, 044702.

- [43] N. Shibayama, H. Maekawa, Y. Nakamura, Y. Haruyama, M. Niibe, S. Ito, *ACS Appl. Mater. Interfaces* **2020**, *12*, 50187.
- [44] W. H. Nguyen, C. D. Bailie, E. L. Unger, M. D. McGehee, *J. Am. Chem. Soc.* **2014**, *136*, 10996.
- [45] S. Wu, W. Wang, M. Li, L. Cao, F. Lyu, M. Yang, Z. Wang, Y. Shi, B. Nan, S. Yu, Z. Sun, Y. Liu, Z. Lu, *Nat. Commun.* **2016**, *7*, 13318.
- [46] A. Chernenkaya, A. Morherr, S. Backes, W. Popp, S. Witt, X. Kozina, S. A. Nepijko, M. Bolte, K. Medjanik, G. Öhrwall, C. Krellner, M. Baumgarten, H. J. Elmers, G. Schönhense, H. O. Jeschke, R. Valentí, *J. Chem. Phys.* **2016**, *145*, 034702.
- [47] R. Schölin, M. H. Karlsson, S. K. Eriksson, H. Siegbahn, E. M. J. Johansson, H. Rensmo, *J. Phys. Chem. C* **2012**, *116*, 26300.
- [48] A. Braun, A. Kubatova, S. Wirick, S. B. Mun, *J Electron Spectros Relat Phenomena* **2009**, *170*, 42.
- [49] K. Seki, H. Ishii, *J Electron Spectros Relat Phenomena* **1998**, *88–91*, 821.
- [50] H. Ishii, K. Seki, *IEEE Trans. Electron Devices* **1997**, *44*, 1295.
- [51] B. Ravel, M. Newville, *J Synchrotron Radiat* **2005**, *12*, 537.
- [52] D. J. F. M. J. Frisch, G. W. Trucks, H. B. Schlegel, G. E. Scuseria, M. A. Robb, J. R. Cheeseman, G. Scalmani, V. Barone, G. A. Petersson, H. Nakatsuji, X. Li, M. Caricato, A. Marenich, J. Bloino, B. G. Janesko, R. Gomperts, B. Mennucci, H. P. Hratchian, J. V. Ort, *Gaussian 09*, Gaussian Inc, Wallingford CT, **2016**.